Depinning phase transition of antiferromagnetic skyrmions with quenched disorder

M. K. Wen,[1] L. Xiong,[2,1,*] and B. Zheng ![ORCID][2,1,3,†]

[1]*Department of Physics, Zhejiang University, Hangzhou 310027, People's Republic of China*
[2]*School of Physics and Astronomy, Yunnan University, Kunming 650091, People's Republic of China*
[3]*Collaborative Innovation Center of Advanced Microstructures, Nanjing University, Nanjing 210093, People's Republic of China*

Antiferromagnetic skyrmions are considered to be promising information carriers due to their attractive properties. Therefore, the pinning phenomenon of antiferromagnetic skyrmions is of great significance. With the Landau-Lifshitz-Gilbert equation, we simulate the nonstationary dynamic behaviors of skyrmions driven by currents in a chiral antiferromagnetic thin film with quenched disorder. Based on the dynamic scaling forms, the critical current and static and dynamic critical exponents of the depinning phase transition are accurately determined. A theoretical analysis using Thiele's approach is presented in comparison with the numerical simulation. Unlike the ferromagnetic skyrmions, the critical current of the antiferromagnetic skyrmions is very sensitive to a small nonadiabatic coefficient. This is important for manipulating antiferromagnetic skyrmions and designing novel information processing devices.

I. INTRODUCTION

Skyrmions are topologically protected objects in chiral magnetic materials [1–4]. It is strongly believed that they have potential applications for information storage and processing because of their rich topological characteristics [5]. Skyrmions in ferromagnetic materials have been intensively studied experimentally and theoretically in the past decade, including studies on the current-driven dynamics, the extralow depinning current, and possible room-temperature stability [6–8]. Nevertheless, the progress on antiferromagnetic skyrmions is still limited. Antiferromagnetic materials are outstanding candidates for the next generation of spintronic applications for their superior properties, such as the robustness against the perturbation from magnetic fields, the absence of production of parasitic stray fields, and the ultrafast dynamics in the terahertz range [9,10]. In spite of these advantages, the absence of a net magnetic moment makes both the detection and the manipulation of antiferromagnetic moments intrinsically difficult in conventional manners. However, the detection of the antiferromagnetic ordering was recently realized based on the anisotropic magnetoresistance and spin pumping effect [11–17]. The current-driven manipulation of the Néel order was also predicted theoretically and confirmed experimentally [18–21]. Following the development of these experimental technologies, the research prospect of antiferromagnetic skyrmions has been greatly expanded.

Antiferromagnetic skyrmions are considered to be futuristic ultrahigh-density information carriers [22]. The Dzyaloshinskii-Moriya (DM) interaction is essential for the formation and stability of skyrmions, especially for small size

skyrmions [22]. It has been observed that the DM interaction is more common in antiferromagnetic materials than in ferromagnetic ones [23]. The absence of the gyroscopic force and the stray field make the antiferromagnetic skyrmions more suitable information carriers [24]. With a driving current, skyrmions in antiferromagnetic materials can move strictly along the current direction without the Hall effect at a high velocity of the order of kilometers per second [23]. The most recent research shows that the antiferromagnetic skyrmions can be experimentally realized [25], which represents an important step towards the implementation of the antiferromagnetic skyrmions in spintronic devices.

The manipulation of the antiferromagnetic skyrmions is one of the most important topics. Previous studies have mainly focused on a small range of the skyrmion velocity and rarely dealt with disorder [26–28]. The systematic study of the current-driven dynamics of the antiferromagnetic skyrmions with quenched disorder is significant both fundamentally and practically. In particular, the pinning phenomenon is not avoidable in the application of skyrmions as information carriers. In ferromagnetic spintronics, the pinning behavior of an individual skyrmion was investigated [22,29,30], and the collective motion of skyrmions in a disordered film was recently explored [31–34]. However, a deep understanding of the pinning phenomenon of skyrmions in antiferromagnetic materials has still not yet been achieved.

Due to critical slowing down, the numerical simulation of the stationary state around a continuous phase transition is very difficult. The dynamic approach in the nonstationary state was recently explored for the depinning phase transitions of the ferromagnetic domain walls and skyrmions [35–39]. Because the measurements are carried out in the short-time regime of the dynamic evolution without reaching the stationary state, such methods are very efficient in dealing with dynamic phase transitions. The simulation of the

---
[*]xionglong@zju.edu.cn
[†]zhengbo@zju.edu.cn

antiferromagnetic skyrmions is, however, more complicated than the ferromagnetic ones, and one needs to consider the sublattice structure and antiferromagnetic frustration [40,41].

In the present work, we study the current-driven motion of the antiferromagnetic skyrmions with quenched disorder, and a second-order depinning phase transition is detected. Based on the Landau-Lifshitz-Gilbert (LLG) equation, we perform the numerical simulations of an antiferromagnetic film for the dynamic relaxation processes around the phase transition to determine the critical current u_c and the critical exponents. A theoretical analysis of the Thiele equation is also presented for comparison with the numerical results. The model and the equation of motion are described in Sec. II, the scaling analysis and a theoretical approach are presented in Sec. III, and the numerical simulations are performed in Sec. IV. The conclusion is given in Sec. V.

II. THE MODEL

We consider an antiferromagnetic film in the xy plane with a perpendicular disorder. The Hamiltonian of the classical Heisenberg model is given as

$$\mathcal{H} = -J \sum_{\langle i,j \rangle} \boldsymbol{m}_i \cdot \boldsymbol{m}_j + \sum_{\langle i,j \rangle} \boldsymbol{D} \cdot (\boldsymbol{m}_i \times \boldsymbol{m}_j)$$
$$- K \sum_{i \in \Lambda} (m_i^z)^2 - \sum_i \boldsymbol{B}_{sg} \cdot \boldsymbol{m}_i, \tag{1}$$

where $\boldsymbol{m}_i$ represents the local magnetic moment normalized as $|\boldsymbol{m}_i| = 1$ and $\langle i, j \rangle$ denotes the summation over the nearest neighbors. The terms on the right-hand side are the exchange interaction, the interfacial DM interaction, the uniaxial anisotropic disorder, and the Zeeman-like staggered field along the z axis. The staggered field is applied due to the opposite magnetization on the two sublattices of the antiferromagnetic materials [42]. Generically, there are two possible ways of inducing this staggered field in different materials such as Cr_2O_3 [43,44] and CuMnAs [18]. Here J is the antiferromagnetic exchange coupling. In this paper, $J = -1$ meV is fixed, and $|J|$ is used to be the unit of other parameters. D is the DM interaction strength, and $\boldsymbol{B}_{sg}$ denotes the staggered magnetic field along the z axis. In order to stabilize the skyrmions, the DM interaction strength and the staggered field are taken to be $D/|J| = 0.4$ and $B_{sg}/|J| = 0.04$, respectively. K is the uniaxial anisotropy constant with the easy axis along the z direction, and Λ is a set of random sites. The density of the random sites and the strength of the disorder are taken to be $\rho = 0.1$ and $K/|J| = 1$.

For comparison, we have additionally investigated the random-field and random-bond disorders. In both cases, we set the anisotropy constant $K = 0$. The random-field disorder is introduced by adding a new term to the Hamiltonian in Eq. (1),

$$\mathcal{H}_{\text{dis},h} = - \sum_{i \in \Lambda'} \boldsymbol{h}_i \cdot \boldsymbol{m}_i, \tag{2}$$

where $\boldsymbol{h}_i$ is the internal random field. The direction of the random field $\boldsymbol{h}_i$ is randomly set on the unit sphere, while the amplitude $|\boldsymbol{h}_i|$ of the random field is uniformly distributed within an interval $[0, \Delta]$, with $\Delta = 0.4$. Λ' is a set of

random sites, and the density of the random sites is 0.5. The random-bond disorder is set by changing the first term of the Hamiltonian in Eq. (1) to

$$\mathcal{H}_{\text{dis},j} = - \sum_{\langle i,j \rangle} J_{ij} \boldsymbol{m}_i \cdot \boldsymbol{m}_j, \tag{3}$$

where $J_{ij} = J$ for 80% bonds and $J_{ij} = 0.1J$ for 20% bonds.

The current-driven dynamical behavior of the magnetic skyrmions is described by the LLG equation including the spin-transfer torque (STT) interactions,

$$\frac{d\boldsymbol{m}}{dt} = -\gamma \boldsymbol{m} \times \boldsymbol{H}_{\text{eff}} + \alpha \boldsymbol{m} \times \frac{d\boldsymbol{m}}{dt}$$
$$- (\boldsymbol{u} \cdot \nabla)\boldsymbol{m} + b\boldsymbol{m} \times (\boldsymbol{u} \cdot \nabla)\boldsymbol{m}, \tag{4}$$

where $\boldsymbol{m}$ just denotes $\boldsymbol{m}_i$ in Eq. (1), γ is the gyromagnetic ratio, and α is the Gilbert damping constant. The effective magnetic field H_{eff} acting on $\boldsymbol{m}$ is computed from

$$\boldsymbol{H}_{\text{eff}} = -\frac{1}{\hbar\gamma} \frac{\partial \mathcal{H}}{\partial \boldsymbol{m}}, \tag{5}$$

which contains the contributions from the exchange interaction, DM interaction, anisotropic disorder, and Zeeman-like field. The last two terms in Eq. (4) describe the STT effect from the coupling between the spin-polarized electric current and the local magnetization. $\boldsymbol{u}$ is the current vector with the amplitude $u = pa^3j/2eM$, where p is the spin polarization rate, a is the lattice constant, M is the magnitude of the local magnetic moment, and j is the magnitude of the spin-polarized electric current. The direction of the current vector $\boldsymbol{u}$ is set along the x direction. b is the nonadiabatic STT coefficient. As explained in the Supplemental Material of Ref. [23], the STTs are applied to each sublattice independently; that is, the gradients of $\boldsymbol{m}$ in Eq. (4) are taken only within the same sublattice. The unit of length is the lattice constant $a = 1$ nm. The time t and the current density j are in units of $\hbar/J \simeq 0.66$ ps and $2e|\boldsymbol{m}|J/Pa^2\hbar \simeq 1.2 \times 10^{12}$ Am^{-2}, respectively, with the spin polarization $P = 0.4$.

The LLG equation is numerically integrated using a fourth-order Rung-Kutta scheme. Our simulations were mainly performed on a magnetic square lattice at zero temperature with lattice size $L = 288$. A simulation of a larger size, $L = 432$, was also performed to confirm that the finite-size effect is negligibly small. In the nonstationary dynamic approach, the measurements are carried out in the short-time regime of the dynamic evolution when the spatial correlation length is still small. Therefore, these lattice sizes are sufficiently large to avoid the finite-size effect. The periodic boundary condition is used in both the x and y directions. The initial state is a perfect triangular antiferromagnetic skyrmion crystal with 256 skyrmions, which is prepared using a replica Monte Carlo simulation [31,45,46]. Then the steady current is applied in the x direction, and the relaxation dynamics is simulated with the LLG equation. Due to the topological protection, a skyrmion keeps the topological structure unless the driving current or the disorder goes beyond a certain threshold. The maximum time of the simulations is set to $t_{\max} = 20\,000$ to observe the dynamic scaling behavior. The time step in the simulations is $\Delta t = 0.1$, and extra simulations with a smaller time step $\Delta t = 0.05$ were performed to confirm the accuracy

of the results. The total number of samples for quenched disorder is about 10 000 to ensure reasonably small statistical errors.

III. THEORY

A. Scaling analysis

The topological charge of an antiferromagnetic skyrmion is defined as

$$Q^{(k)} = -\frac{1}{4\pi} \int d^2r (\partial_x \boldsymbol{m}^{(k)} \times \partial_y \boldsymbol{m}^{(k)}) \cdot \boldsymbol{m}^{(k)}, \quad k = 1, 2, \quad (6)$$

where k labels the sublattices. The antiferromagnetic skyrmion is composed of two topological objects with opposite winding numbers, i.e., $Q^{(k)} = \pm 1$. The strong coupling between the sublattices leads to a perfect cancellation of two opposite Hall forces; therefore, the antiferromagnetic skyrmion does not present a transverse motion. Alternatively, one can also directly define the topological charge Q of the antiferromagnetic Néel order parameter $\boldsymbol{l}(\boldsymbol{r}, t) = \boldsymbol{m}^{(1)}(\boldsymbol{r}, t) - \boldsymbol{m}^{(2)}(\boldsymbol{r}, t)$ by replacing $\boldsymbol{m}^{(k)}$ with $\boldsymbol{l}(\boldsymbol{r}, t)$ in Eq. (6). In this notation, the topological character of the antiferromagnetic skyrmion is represented by the topological charge $Q = 1$. If there are N antiferromagnetic skyrmions, the topological charge Q is equal to N.

The velocity of the skyrmions can be measured through the emergent electric field induced by the moving skyrmions in ferromagnetic materials. It has been shown that the swirling structure of a skyrmion induces a magnetic field $\boldsymbol{B}^e$, while a skyrmion lattice drifting with a velocity $\boldsymbol{v}_d$ induces an electric field $\boldsymbol{E}^e = -\boldsymbol{v}_d \times \boldsymbol{B}^e$ [8,47]. To evaluate the velocity of the moving skyrmions, one may measure the emergent electric field [31,47]

$$E_\mu^e = \int d^2r (\partial_\mu \boldsymbol{m} \times \partial_t \boldsymbol{m}) \cdot \boldsymbol{m}, \qquad \mu = x, \ y. \quad (7)$$

We introduce an analogy to evaluate the antiferromagnetic skyrmion velocity by measuring the emergent electric field induced by the Néel order parameter. The only nonzero component of the electric field is along the y direction. In analogy to Eq. (7), the magnitude of the electric field is expressed as

$$E^e = \int d^2r (\partial_y \boldsymbol{l} \times \partial_t \boldsymbol{l}) \cdot \boldsymbol{l}. \quad (8)$$

The emergent magnetic field $\boldsymbol{B}^e = (0, 0, Q)$ is along the z direction in our simulation. The average velocity of the skyrmions is thus

$$v = -\langle E^e/Q \rangle, \quad (9)$$

where the velocity v is along the x direction and $\langle \cdots \rangle$ represents the statistical average of all samples.

With quenched disorder, the collective motion of antiferromagnetic skyrmions driven by the electric current exhibits a dynamic depinning phase transition. Assuming the phase transition is second order, the dynamic evolution of the order parameter $v(t)$ should obey the dynamic scaling theory supported by the renormalization-group calculations [48–50]. For a simulation box with a size L, the critical dynamic scaling form for the average velocity of skyrmions is described by

$$v(t, \tau, L) = \lambda^{-\beta/\nu} v(\lambda^{-z}t, \lambda^{1/\nu}\tau, \lambda^{-1}L), \quad (10)$$

where λ is an arbitrary scale factor, u_c is the critical current, $\tau = (u - u_c)/u_c$ is the reduced current, β and ν are the static exponents, and z is the dynamic exponent. Putting $\lambda \sim t^{1/z}$ in Eq. (10), we obtain

$$v(t, \tau, L) = t^{-\beta/\nu z} v(1, t^{1/\nu z}\tau, t^{-1/z}L). \quad (11)$$

In the macroscopic short-time regime far from the stationary state, the spatial correlation length $\xi(t) \sim t^{1/z} \ll L$, and the finite-size effect is small and ignorable. This leads to

$$v(t, \tau) = t^{-\beta/\nu z} G(t^{1/\nu z}\tau), \quad (12)$$

where $G(t^{1/\nu z}\tau)$ is the scaling function of the skyrmion velocity. In the limit of $t \to \infty$, $G(x) \to x^\beta$, and $v(t, \tau) \sim \tau^\beta$. At the depinning transition current, i.e., $\tau = 0$, $G(0)$ is independent of the time t, and the scaling form reduces to a power-law behavior,

$$v(t) \sim t^{-\beta/\nu z}. \quad (13)$$

The critical current u_c can be determined by searching for the best power-law behavior of $v(t)$. We can then measure the exponent $\beta/\nu z$ by a power-law fitting to Eq. (13). To calculate $1/\nu z$, one simply derives from Eq. (12),

$$\frac{\partial \ln v(t, \tau)}{\partial \tau}\Big|_{\tau=0} \sim t^{1/\nu z}. \quad (14)$$

The Binder cumulant of the velocity is defined as

$$v^{(2)}(t) = \frac{\langle v^2(t) \rangle - \langle v(t) \rangle^2}{\langle v(t) \rangle^2}. \quad (15)$$

Based on the finite-size scaling analysis at the critical current, the Binder cumulant should scale as

$$v^{(2)}(t) \sim [\xi(t)/L]^d, \quad (16)$$

where $d = 2$ is the spatial dimension of the antiferromagnetic film. Thus, the spatial correlation length $\xi(t)$ can be computed through $v^{(2)}(t)$ up to a constant factor, and the dynamic exponent z can be independently determined. To estimate the constant factor, one could calculate the correlation function of the line electric field in the x direction in analogy to the height correlation function [51]. The correlation function is defined as

$$C(r, t) = \langle [E^e(x + r, t) - E^e(x, t)] \rangle, \quad (17)$$

where $E^e(x, t) = \int dy[\partial_y \boldsymbol{l}(x, y, t) \times \partial_t \boldsymbol{l}(x, y, t)] \cdot \boldsymbol{l}(x, y, t)$ is the emergent field in Eq. (8) integrating only along the y direction at position x. At the critical current, $C(r, t)$ obeys the scaling behavior [51,52],

$$C(r, t) \sim \tilde{C}[r/\xi(t)] \sim \{\tanh[r/\xi(t)]\}^a. \quad (18)$$

By fitting this scaling form, the correlation length $\xi(t)$ can be calculated, and the resulting $\xi(t)$ is in good agreement with the one obtained in Eq. (16). Thus, one estimates that $[v^{(2)}(t)]^{1/d}$ is proportional to $\xi(t)/L$ with a factor of about 1.5.

B. Theoretical solution

We investigate the theoretical solution of the critical current u_c through a particle-based model derived from the Landau-Lifshitz-Gilbert equation. With Thiele's approach, the

collective motion of skyrmions is analyzed in the stationary state. A generalized Thiele equation, in which the spin textures of skyrmions are assumed to be rigid, is adopted [53],

$$\boldsymbol{G} \times (\boldsymbol{u} - \boldsymbol{v}_d) + \boldsymbol{\mathcal{D}}(b\boldsymbol{u} - \alpha \boldsymbol{v}_d) + \boldsymbol{F}_{\text{pin}} = 0. \tag{19}$$

Here $\boldsymbol{v}_d$ is the drift velocity of skyrmions in the stationary state, and only the x component of $\boldsymbol{v}_d$ is nonzero because the antiferromagnetic skyrmions move straight without the Hall motion in the perpendicular direction of the driving current. The first term describes the Magnus force, and $\boldsymbol{G}$ is the gyromagnetic coupling vector. An antiferromagnetic skyrmion can be regarded as the nesting of two ferromagnetic skyrmions in each sublattice with opposite topological charges. The opposite Magnus forces acting on each sublattice are perfectly canceled because the two sublattices are strongly coupled together by the exchange coupling J. Thus, there is no Hall effect, and $\boldsymbol{G}$ equals zero. For antiferromagnetic skyrmions, the nonadiabatic coefficient b affects only the motion along the driving current direction because of the absence of the transverse motion, while for the ferromagnetic skyrmions, b does play an important role both along and perpendicular to the current. The second term represents the dissipative force, and the dissipative force tensor $\boldsymbol{\mathcal{D}}$ is given by

$$\mathcal{D}_{\mu\nu} = \iint (\partial_\mu \boldsymbol{m} \cdot \partial_\nu \boldsymbol{m}) dx\, dy. \tag{20}$$

Although the dissipation tensor is not perfectly diagonal when skyrmions are distorted by disorder, the nondiagonal components of the tensor are now neglected in order to simplify the theoretical analysis [45,53]. In the stationary state, we assume that the diagonal components $\mathcal{D}$ remain constant [31].

The pinning force is described by the last term in Eq. (19), which usually takes the form [53]

$$\boldsymbol{F}_{\text{pin}} \sim -4\pi v_{\text{pin}} f(v_d/v_{\text{pin}}) \boldsymbol{v}_d / |\boldsymbol{v}_d|. \tag{21}$$

The strength of $\boldsymbol{F}_{\text{pin}}$ is parametrized by the "pinning velocity" v_{pin}. The function $f(x)$, with $f(x \to 0) = 1$ and $f(x \to \infty) = x^\nu$, describes the nonlinear dependence of the pinning force on the velocity. With the above conditions, Eq. (19) for the antiferromagnetic skyrmions near the critical current can be simplified to a scalar equation,

$$\mathcal{D}(bu - \alpha v_d) - F = 0, \tag{22}$$

where F is a constant denoting the strength of $\boldsymbol{F}_{\text{pin}}$ when $v_d/v_{\text{pin}} \to 0$. Thus, the drift velocity is

$$v_d = \frac{bu}{\alpha} - \frac{F}{\alpha \mathcal{D}}. \tag{23}$$

Without disorder, $v_d = bu/\alpha$ is just the same as that derived from the antiferromagnetic analogs of the LLG equation [23,54]. With disorder, we obtain the critical current u_c by setting $v_d = 0$,

$$u_c = \frac{F}{\mathcal{D}b}, \tag{24}$$

which is inversely proportional to the nonadiabatic coefficient b but not affected by the damping constant α.

IV. SIMULATIONS

We first simulate the dynamic behavior of the antiferromagnetic skyrmions on a lattice of $L = 288$ without disorder, i.e., with the zero density of the random sites, $\rho = 0$. The simulations are performed with nonadiabatic coefficient $b = 0.005$, 0.05, and 0.2. As shown in Fig. 1(a), the antiferromagnetic skyrmion velocity v_d is proportional to u in the small u region, which is in agreement with the theoretical result $v_d = bu/\alpha$, based on the Thiele equation [23,54]. With a large driving current u, the skyrmions are contracted in the x direction and stretched along the y direction and will be gradually distorted to the stripes. The skyrmion velocity is smaller than the theoretical one in this case. When u exceeds a certain threshold, the topological structure of the skyrmions will be thoroughly corrupted, and the dynamic system will experience a transition from the antiferromagnetic skyrmions to the helical states. This phenomenon is illustrated in Fig. 1(b), and the topological charge Q undergoes an abrupt change as u increases. The threshold current for $Q = 0$ decreases with b.

Then we investigate how the threshold current of this skyrmion-helical transition changes with the strength of the disorder K. The nonadiabatic coefficient $b = 0.05$ and the density of the random sites $\rho = 0.1$ are fixed. In the simulations, it was confirmed that the finite-size effect for $L = 288$ is already small. In Fig. 1(c), the u-K diagram of the topological charge Q is displayed. The threshold current for $Q = 0$ increases with K. Q experiences an abrupt change at the critical point without disorder. For a smaller K, Q decreases rapidly when u increases in the transition regime. For a larger K, the decreasing of Q slows down. Disorder prevents the transition from the skyrmion to the helical state by producing an intermediate state between the skyrmion and helical states. In fact, various physical behaviors in the structural transition regime exist, particularly in the presence of disorder and in a high-velocity regime. We will not go into detail in the present work.

Next, we focus on the pinning-depinning phase transition of the antiferromagnetic skyrmions with disorder. For a very small b, the phase transition may not occur in the regime in which skyrmions are not distorted by the driving current. With the chosen parameters in this work, the critical current u_c for $b = 0.005$ will drop into the regime where skyrmions already deform to the stripe states. Therefore, our simulations are performed with nonadiabatic coefficients $b = 0.05$, 0.2, 0.5, and 1. From Eq. (23), the antiferromagnetic skyrmions cannot move without a nonadiabatic STT, i.e., the critical current $u_c \to +\infty$ for $b = 0$, and this is significantly different from the ferromagnetic skyrmions. Simulations with and without disorder for $b = 0$ were also performed to confirm it.

In Fig. 2, the initial state of a triangular antiferromagnetic skyrmion crystal is plotted. The lattice size is $L = 288$, and there are 256 skyrmions in total. The dynamic scaling form in Eq. (12) also holds for other initial states, such as those with randomly distributed skyrmions. Different initial states affect only the microscopic behavior at the beginning stage of the time evolution, and the time-dependent velocities tend to exhibit the same universal dynamic behavior after a macroscopic short-time scale t_{mic}. The initial state of the triangular crystal is adopted because it is the ground state and has a
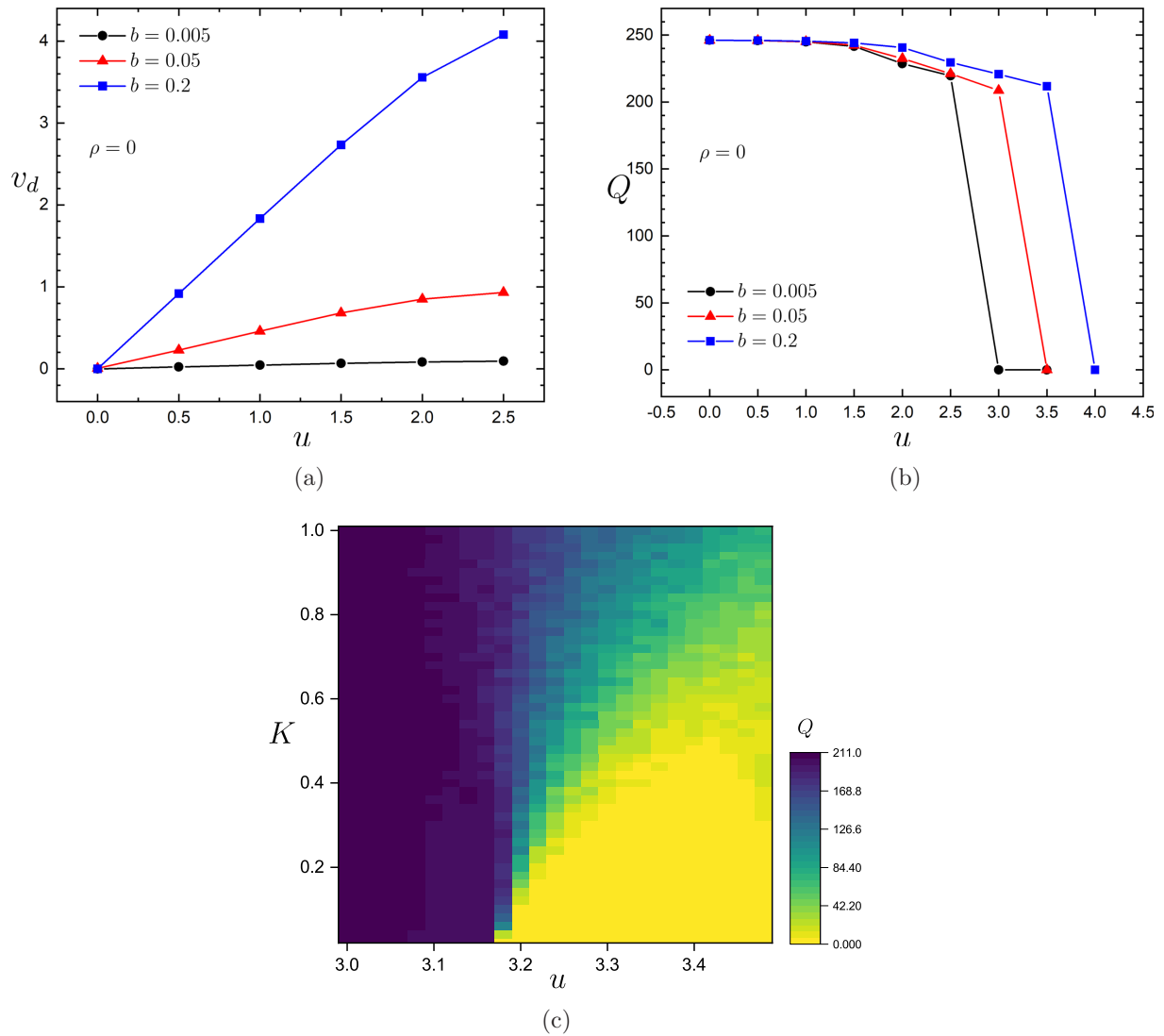
FIG. 1. (a) The velocity v_d of the antiferromagnetic skyrmions versus the driving current u with different values of the nonadiabatic STT coefficient b without disorder. (b) The topological charge Q of the Néel order versus the driving current u without disorder. (c) The u-K phase diagram of the topological charge Q with the fixed disorder density $\rho = 0.1$ and nonadiabatic coefficient $b = 0.05$.
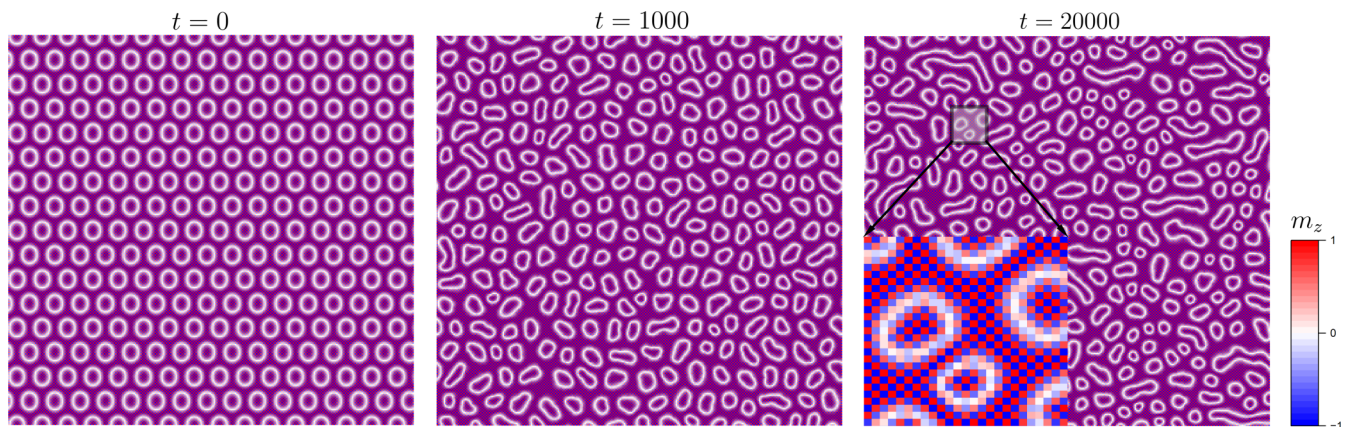

FIG. 2. The initial state with a perfect triangular antiferromagnetic skyrmion crystal and the time evolution of the spin configuration m_z for $b = 0.05$ and $\rho = 0.1$ at the critical current $u_c = 0.750$. The color represents the value of m_z. The inset in the $t = 20\,000$ plot is a zoomed-in portion to show the antiferromagnetic structure of $\boldsymbol{m}$.
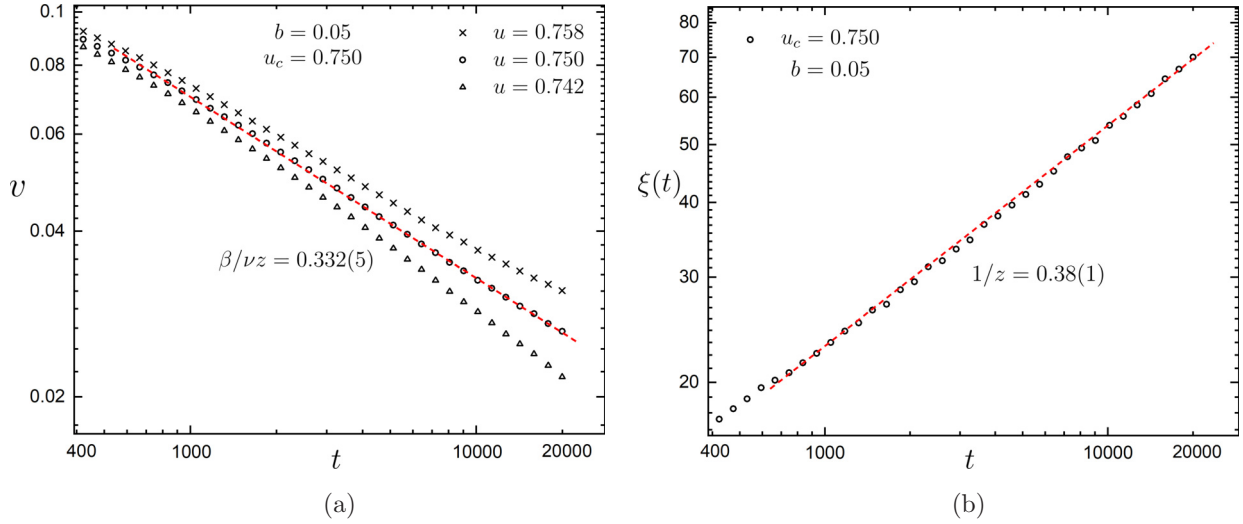
FIG. 3. (a) The antiferromagnetic skyrmion velocity $v(t)$ is displayed with $b = 0.05$ for different values of the driving current u on a log-log scale. (b) The correlation length $\xi(t)$ is plotted. Dashed lines show the power-law fits.

smaller t_{mic}. The time evolution of the skyrmion structure in an antiferromagnetic thin film with quenched disorder is also plotted at the critical current $u_c = 0.750$ for $b = 0.05$. As time evolves, skyrmions may be stretched along the moving direction, while the crystal structure of the skyrmions gradually deforms to a glasslike state, which is similar to skyrmions in ferromagnetic materials [31,55]. In this many-skyrmion system, the skyrmion-skyrmion interaction provides a repulsive force between skyrmions, and it leads to skyrmions stabler than a single skyrmion. More importantly, the collective correlation between skyrmions caused by the skyrmion-skyrmion interaction ensures that the depinning phase transition is in the thermodynamic sense. According to our simulation results of a single skyrmion moving in the disordered environment, it experiences a first-order-like transition, rather than a second-order phase transition in the thermodynamic sense.

In Fig. 3(a), the skyrmion velocity v is displayed for different values of the driving current u. In the long-time regime, the velocity will drop down for a small u, while it approaches a constant for a larger u. Searching for the best power-law behavior, one locates the critical current $u_c = 0.750(1)$. At the critical current, the velocity evolves with time in a power law, which indicates a divergent correlating time, and the stationary state can never be reached in the infinite limit of the lattice size L. $u = 0.742$ and $u = 0.758$ are close to the critical current $u_c = 0.750(1)$. Below the critical current, the skyrmion system at $u = 0.742$ will relax to the pinned phase after a long time, and the velocity will finally go to zero. Above the critical current, the skyrmion system at $u = 0.758$ will finally reach the depinning state with a nonzero velocity. From the slope of the critical curve $u = 0.750$, one measures the critical exponent $\beta/\nu z = 0.332(5)$ according to Eq. (13). The errors include both the statistical ones and the fluctuations along the time direction. In Fig. 3(b), the correlation length $\xi(t)$ exhibits a power-law behavior at u_c. One obtains the critical exponent $1/z = 0.38(1)$ from the slope of the curve on a log-log scale. The correlation length $\xi(t)$ increases from 0 to about 70 at $t = 20\,000$. $\xi(t)$ is much smaller than the lattice size of $L = 288$ and about seven times the average

skyrmion diameter. Therefore, the short-time dynamic scaling form holds, and the finite-size effect is negligibly small.

To calculate the logarithmic derivative $\partial_\tau \ln v(t, \tau)$, we quadratically interpolate $v(t, \tau)$ between $u = 0.742$ and $u = 0.758$ with the data in Fig. 3(a). A power-law behavior is observed at u_c in Fig. 4(a), and the slope of the curve yields the critical exponent $1/\nu z = 0.44(2)$. In Fig. 4(b), the critical current u_c measured from the LLG simulation is plotted versus the nonadiabatic coefficient b, compared with the theoretical solution in Eq. (24). To fit the curve, the constant $F/\mathcal{D}$ in Eq. (24) is estimated from the simulation result of the critical current u_c at $b = 0.05$. The numerical and theoretical results agree very well with each other. The critical current u_c of the skyrmions in ferromagnetic materials has been reported to be insensitive to the nonadiabatic coefficient b in the small b region [31,45], while u_c for the antiferromagnetic skyrmions is just the opposite, very sensitive to a small b. This is in agreement with the theoretical expressions of critical current u_c in ferromagnetic and antiferromagnetic materials. From the theoretical solution of u_c for the ferromagnetic skyrmions [31], $u_c = \sqrt{\mathcal{A}^2/(\mathcal{D}^2 b^2 + \mathcal{G}^2)}$, the extra term $\mathcal{G}^2$ makes u_c less sensitive to b, compared with the antiferromagnetic case in Eq. (24). The sensitivity of u_c to a small b in antiferromagnetic materials is apparently associated with the intrinsic pinning of the antiferromagnetic skyrmions at $b = 0$. The intrinsic pinning means that the antiferromagnetic skyrmions cannot be driven without the nonadiabatic STT, whether disorder exists or not. This implies that the critical current $u_c \to \infty$ with $b = 0$. Hence, there is a rapid change in u_c when $b \to 0$. The intrinsic pinning could be understood from the Thiele equation. For antiferromagnetic materials without disorder, the first and third terms in Eq. (19) are canceled; thus, $\mathbf{v}_d$ goes to zero at $b = 0$. The sensitivity of the critical current of the antiferromagnetic skyrmions to a small nonadiabatic coefficient b provides extra flexibility in potential applications. For a very large nonadiabatic coefficient, we have simulated the case of $b = 10$, and the critical current u_c is about 0.0037. The adiabatic term in Eq. (4) is very small around such a small critical current u_c. The simulation result shows that the phase
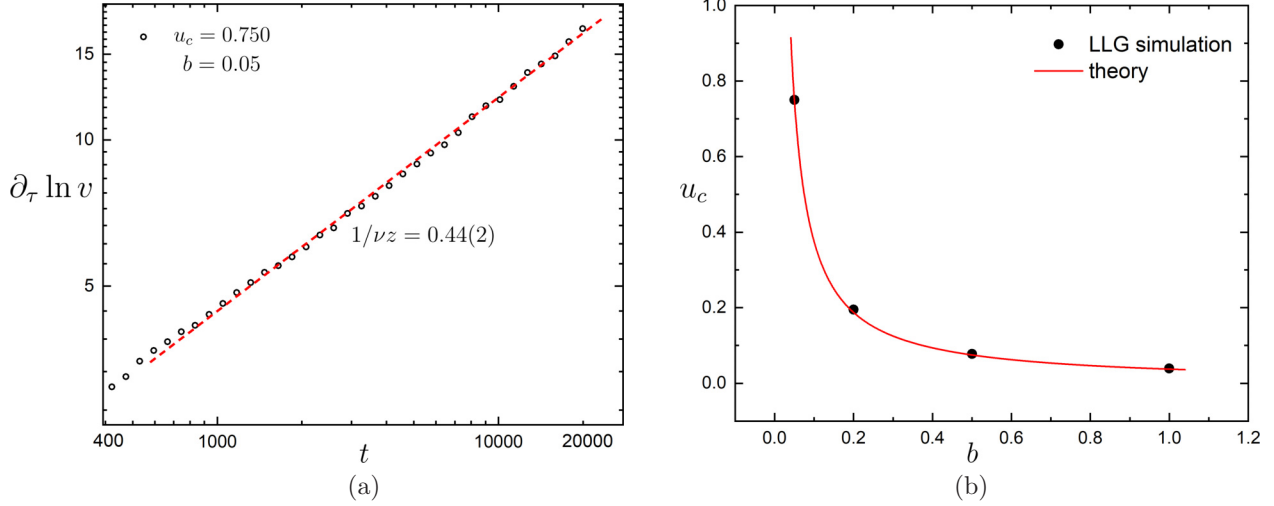
FIG. 4. (a) The logarithmic derivative $\partial_\tau \ln v(t, \tau)$ versus time t at the critical current $u_c = 0.750$. The dashed line shows the power-law fit. (b) The critical current u_c from the numerical simulation and theoretical analysis.

transition remains second order, and the relation of the critical current in Eq. (24) holds in the small adiabatic STT regime.

Based on the dynamic scaling form far from equilibrium, all the critical exponents for the depinning phase transition of the antiferromagnetic skyrmions are accurately measured for different values of the nonadiabatic coefficient b and are summarized In Table I. Although the critical current varies significantly, the critical exponents β, ν, and z remain basically unchanged within error, at least for $b > 0.05$. For the ferromagnetic skyrmions, the critical exponents are anisotropic in two directions due to the Hall effect, and in particular, there is a crossover from the universality class of the adiabatic STT to that of the nonadiabatic STT in the direction parallel to the driving current, with β changing from 2 to 1 [31]. However, β is not equal to 1 with any nonadiabatic coefficient b for the antiferromagnetic skyrmions, which indicates a nonlinear relation between the velocity and the driving current near the depinning transition. The antiferromagnetic skyrmions exhibit a depinning phase transition only in the parallel direction, with a strong universality class for a nonadiabatic coefficient $b > 0.05$. Similar to the antiferromagnetic skyrmions, vortices are another type of topological texture without the Magnus force. The static critical exponents for the elastic and plastic depinning transitions of vortices are, respectively, $\beta = 0.29(3)$ and $\beta = 1.3(1)$ [31,56,57], which are also very different from $\beta = 0.83(5)$ for the antiferromagnetic skyrmions.

The critical behavior may be changed by the pinning force. According to the stationary state analysis in Eq. (24), the pinning force strength F is proportional to u_c. In Table II, the critical exponents at $b = 0.5$ for different disorder strengths and densities are summarized in order of the critical current u_c. We choose the same b so that u_c may depict the pinning force strength. The critical exponents slightly vary for weaker pinning forces and are stabilized for strong pinning forces with $u_c \geqslant 0.0774$. This is qualitatively in agreement with the critical behavior of ferromagnetic skyrmions [31]. For comparison, we have also investigated the random-bond and random-field disorders, which are described in Eqs. (2) and (3).

In Table III, the critical exponents at $b = 0.5$ for different disorder types are summarized. The critical exponents of the random-field disorder are almost the same as those of the anisotropy disorder, except that the dynamic exponent z is slightly bigger. These two cases likely belong to the same universality class. For the random-bond disorder, even with the disorder strength at its largest limit such that the skyrmions would not be destroyed, the pinning force is still very weak. The static exponent ν is close to that of the strong anisotropy disorder, while the static exponent β and the dynamic exponent z of the random-bond disorder are very different,

TABLE I. The critical current and critical exponents for the depinning phase transition of skyrmions in an antiferromagnetic thin film with different values of the nonadiabatic coefficient b.

b	u_c	β	ν	z
0.05	0.750(1)	0.75(3)	0.86(4)	2.63(3)
0.2	0.1929(2)	0.83(5)	0.88(6)	2.31(5)
0.5	0.0774(3)	0.83(5)	0.88(5)	2.35(6)
1	0.0385(1)	0.84(4)	0.87(5)	2.33(8)

TABLE II. The critical current and critical exponents for the depinning phase transition of skyrmions in an antiferromagnetic thin film for different disorder strengths K and disorder densities ρ at a nonadiabatic coefficient $b = 0.5$. The rows are sorted by the critical current u_c.

K	ρ	u_c	β	ν	z
1.0	0.05	0.0444(1)	0.89(4)	0.82(4)	2.43(2)
0.75	0.1	0.0471(2)	0.90(2)	0.84(3)	2.34(6)
1.0	0.1	0.0774(3)	0.83(5)	0.88(5)	2.35(6)
1.0	0.15	0.110(1)	0.82(3)	0.98(3)	2.43(4)
1.25	0.1	0.117(1)	0.84(4)	0.98(5)	2.44(7)

TABLE III. The critical current and critical exponents for the depinning phase transition of skyrmions in an antiferromagnetic thin film for different types of disorder with a nonadiabatic coefficient $b = 0.5$. The random-field and random-bond disorders are described in Eqs. (2) and (3). The rows are sorted by the critical current u_c.

Disorder	u_c	β	ν	z
Random bond	0.01105(2)	1.41(4)	1.00(3)	1.67(5)
Random field	0.0475(2)	0.88(4)	0.87(4)	2.50(4)
Anisotropy	0.0774(3)	0.83(5)	0.88(5)	2.35(6)

obviously belonging to another universality class. In previous studies for both the elastic model and the Ising model, the random-bond and random-field depinning universality classes merge into the same one [58–60]. The critical exponents may vary in the weak disorder region, whereas they usually tend to be stable when the disorder is strong [60,61]. In our simulation of the Heisenberg model, the random-bond disorder is already in the strong region, and an even larger disorder will destroy the structure of the skyrmion.

A different universality class for the random-bond disorder in the Heisenberg model may arise from two possible origins. First, the LLG simulation involves more detailed microscopic structures and interactions, such as magnetic moment precession. The Hamiltonian is not introduced directly in the LLG equation, but the corresponding effective field is included. The random-bond disorder acts on the system as a correction to the Laplacian of the local $\boldsymbol{m}$, which is distinct from the Ising model. On the other hand, the random field and random anisotropy are similar to those in the Ising model. Second and more importantly, the previous simulation results for the depinning phase transition in magnetic systems are mainly for ferromagnetic materials. However, the critical behavior of ferromagnets and antiferromagnets can be quite different. For instance, the critical exponents and the universality classes are different in order-disorder transitions because of the different exchange interactions [62,63]. In antiferromagnetic

materials, the sublattices are coupled together through the exchange interaction. Therefore, the random-bond disorder significantly affects the antiferromagnetism of the material, whereas the random field and random anisotropy do not. Thus, the random-bond disorder induces a different universality class for the depinning phase transition of skyrmions.

V. CONCLUSION

In summary, we have investigated the dynamical behaviors of antiferromagnetic skyrmions with the LLG equation. A structural transition from antiferromagnetic skyrmions to helical states is observed. The threshold current for $Q = 0$ decreases with the nonadiabatic coefficient b. We then focused on the numerical simulations of the nonstationary dynamic behavior of skyrmions driven by currents in a chiral antiferromagnetic thin film with quenched disorder. A depinning phase transition is detected, which is second disorder. Based on the dynamic scaling forms, the critical current and static and dynamic critical exponents were precisely measured. The depinning phase transition of the antiferromagnetic skyrmions belongs to a new universality class. Our nonstationary dynamic approach is efficient because it does not suffer from critical slowing down. The theoretical solution of the critical current u_c based on the Thiele equation was also presented and agrees well with the numerical simulation. According to our simulation and theoretical results, the critical current u_c of the antiferromagnetic skyrmions is very sensitive to a small nonadiabatic coefficient b, which is different from the ferromagnetic case, and this is important in manipulating antiferromagnetic skyrmions.

ACKNOWLEDGMENTS

[1] A. Bogdanov and A. Hubert, J. Magn. Magn. Mater. **138**, 255 (1994).

[2] U. K. Roessler, A. N. Bogdanov, and C. Pfleiderer, Nature (London) **442**, 797 (2006).

[3] S. Mühlbauer, B. Binz, F. Jonietz, C. Pfleiderer, A. Rosch, A. Neubauer, R. Georgii, and P. Böni, Science **323**, 915 (2009).

[4] X. Z. Yu, Y. Onose, N. Kanazawa, J. H. Park, J. H. Han, Y. Matsui, N. Nagaosa, and Y. Tokura, Nature (London) **465**, 901 (2010).

[5] A. Fert, V. Cros, and J. Sampaio, Nat. Nanotechnol. **8**, 152 (2013).

[6] N. Romming, C. Hanneken, M. Menzel, J. E. Bickel, B. Wolter, K. von Bergmann, A. Kubetzka, and R. Wiesendanger, Science **341**, 636 (2013).

[7] J. Sampaio, V. Cros, S. Rohart, A. Thiaville, and A. Fert, Nat. Nanotechnol. **8**, 839 (2013).

[8] T. Schulz, R. Ritz, A. Bauer, M. Halder, M. Wagner, C. Franz, C. Pfleiderer, K. Everschor, M. Garst, and A. Rosch, Nat. Phys. **8**, 301 (2012).

[9] V. Baltz, A. Manchon, M. Tsoi, T. Moriyama, T. Ono, and Y. Tserkovnyak, Rev. Mod. Phys. **90**, 015005 (2018).

[10] K. Olejník, T. Seifert, Z. Kašpar, V. Novák, P. Wadley, R. P. Campion, M. Baumgartner, P. Gambardella, P. Němec, J. Wunderlich, J. Sinova, P. Kužel, M. Müller, T. Kampfrath, and T. Jungwirth, Sci. Adv. **4**, eaar3566 (2018).

[11] B. G. Park, J. Wunderlich, X. Martí, V. Holý, Y. Kurosaki, M. Yamada, H. Yamamoto, A. Nishide, J. Hayakawa, H. Takahashi, A. B. Shick, and T. Junwirth, Nat. Mater. **10**, 347 (2011).

[12] Y. Y. Wang, C. Song, B. Cui, G. Y. Wang, F. Zeng, and F. Pan, Phys. Rev. Lett. **109**, 137201 (2012).

[13] X. Marti, I. Fina, C. Frontera, J. Liu, P. Wadley, Q. He, R. J. Paull, J. D. Clarkson, J. Kudrnovský, I. Turek, J. Kuneš, D. Yi, J. H. Chu, C. T. Nelson, L. You, E. Arenholz, S. Salahuddin, J. Fontcuberta, T. Jungwirth, and R. Ramesh, Nat. Mater. **13**, 367 (2014).

[14] T. Moriyama, N. Matsuzaki, K. J. Kim, I. Suzuki, T. Taniyama, and T. Ono, Appl. Phys. Lett. **107**, 122403 (2015).

[15] H. V. Gomonay and V. M. Loktev, Phys. Rev. B **81**, 144427 (2010).

[16] R. Cheng, J. Xiao, Q. Niu, and A. Brataas, Phys. Rev. Lett. **113**, 057601 (2014).

[17] E. Gomonay and V. Loktev, Low Temp. Phys. **40**, 17 (2014).

[18] J. Železný, H. Gao, K. Výborný, J. Zemen, J. Mašek, A. Manchon, J. Wunderlich, J. Sinova, and T. Jungwirth, Phys. Rev. Lett. **113**, 157201 (2014).

[19] P. Wadley *et al.*, Science **351**, 587 (2016).

[20] X. Z. Chen, R. Zarzuela, J. Zhang, C. Song, X. F. Zhou, G. Y. Shi, F. Li, H. A. Zhou, W. J. Jiang, F. Pan, and Y. Tserkovnyak, Phys. Rev. Lett. **120**, 207204 (2018).

[21] T. Moriyama, K. Oda, T. Ohkochi, M. Kimata, and T. Ono, Sci. Rep. **8**, 14167 (2018).

[22] N. Nagaosa and Y. Tokura, Nat. Nanotechnol. **8**, 899 (2013).

[23] J. Barker and O. A. Tretiakov, Phys. Rev. Lett. **116**, 147203 (2016).

[24] X. C. Zhang, Y. Zhou, and M. Ezawa, Sci. Rep. **6**, 1 (2016).

[25] S. Gao, H. D. Rosales, F. A. G. Albarracín, V. Tsurkan, G. Kaur, T. Fennell, P. Steffens, M. Boehm, P. Čermák, A. Schneidewind, E. Ressouche, D. C. Cabra, C. Rüegg, and O. Zaharko, Nature (London) **586**, 37 (2020).

[26] T. Dohi, S. DuttaGupta, S. Fukami, and H. Ohno, Nat. Commun. **10**, 5153 (2019).

[27] L. C. Shen, X. G. Li, Y. L. Zhao, J. Xia, G. P. Zhao, and Y. Zhou, Phys. Rev. Appl. **12**, 064033 (2019).

[28] A. Salimath, F. J. Zhuo, R. Tomasello, G. Finocchio, and A. Manchon, Phys. Rev. B **101**, 024429 (2020).

[29] J. V. Kim and M. W. Yoo, Appl. Phys. Lett. **110**, 132404 (2017).

[30] Y. H. Liu and Y. Q. Li, J. Phys.: Condens. Matter **25**, 076005 (2013).

[31] L. Xiong, B. Zheng, M. H. Jin, and N. J. Zhou, New J. Phys. **22**, 033043 (2020).

[32] L. Xiong, B. Zheng, M. H. Jin, and N. J. Zhou, Phys. Rev. B **100**, 064426 (2019).

[33] C. Reichhardt and C. J. O. Reichhardt, New J. Phys. **18**, 095005 (2016).

[34] C. Reichhardt, D. Ray, and C. J. O. Reichhardt, Phys. Rev. B **98**, 134418 (2018).

[35] N. J. Zhou, B. Zheng, and Y. Y. He, Phys. Rev. B **80**, 134425 (2009).

[36] E. V. Albano, M. A. Bab, G. Baglietto, R. A. Borzi, T. S. Grigera, E. S. Loscar, D. E. Rodriguez, M. L. R. Puzzo, and G. P. Saracco, Rep. Prog. Phys. **74**, 026501 (2011).

[37] M. H. Jin, B. Zheng, L. Xiong, N. J. Zhou, and L. Wang, Phys. Rev. E **98**, 022126 (2018).

[38] L. Xiong, B. Zheng, M. H. Jin, L. Wang, and N. J. Zhou, New J. Phys. **20**, 023027 (2018).

[39] M. H. Jin, N. J. Zhou, L. Xiong, and B. Zheng, J. Stat. Mech. (2019) 053303.

[40] M. F. Collins and O. A. Petrenko, Can. J. Phys. **75**, 605 (1997).

[41] K. Y. Jing, C. Wang, and X. R. Wang, Phys. Rev. B **103**, 174430 (2021).

[42] R. Zarzuela, S. K. Kim, and Y. Tserkovnyak, Phys. Rev. B **100**, 100408(R) (2019).

[43] X. He, Y. Wang, N. Wu, A. N. Caruso, E. Vescovo, K. D. Belashchenko, P. A. Dowben, and C. Binek, Nat. Mater. **9**, 579 (2010).

[44] K. D. Belashchenko, O. Tchernyshyov, A. A. Kovalev, and O. A. Tretiakov, Appl. Phys. Lett. **108**, 132403 (2016).

[45] J. Iwasaki, M. Mochizuki, and N. Nagaosa, Nat. Commun. **4**, 1463 (2013).

[46] M. Mochizuki, X. Z. Yu, S. Seki, N. Kanazawa, W. Koshibae, J. Zang, M. Mostovoy, Y. Tokura, and N. Nagaosa, Nat. Mater. **13**, 241 (2014).

[47] W. Koshibae and N. Nagaosa, Sci. Rep. **8**, 6328 (2018).

[48] H. K. Janssen, B. Schaub, and B. Schmittmann, Z. Phys. B **73**, 539 (1989).

[49] B. Zheng, Int. J. Mod. Phys. B **12**, 1419 (1998).

[50] H. J. Luo, L. Schülke, and B. Zheng, Phys. Rev. Lett. **81**, 180 (1998).

[51] M. Jost and K. D. Usadel, Phys. Rev. B **54**, 9314 (1996).

[52] N. J. Zhou and B. Zheng, Phys. Rev. E **82**, 031139 (2010).

[53] K. Everschor, M. Garst, B. Binz, F. Jonietz, S. Mühlbauer, C. Pfleiderer, and A. Rosch, Phys. Rev. B **86**, 054432 (2012).

[54] E. G. Tveten, A. Qaiumzadeh, O. A. Tretiakov, and A. Brataas, Phys. Rev. Lett. **110**, 127208 (2013).

[55] C. Reichhardt, D. Ray, and C. J. Olson Reichhardt, Phys. Rev. Lett. **114**, 217202 (2015).

[56] Y. Fily, E. Olive, N. Di Scala, and J. C. Soret, Phys. Rev. B **82**, 134519 (2010).

[57] N. Di Scala, E. Olive, Y. Lansac, Y. Fily, and J. C. Soret, New J. Phys. **14**, 123027 (2012).

[58] P. Le Doussal, K. J. Wiese, and P. Chauve, Phys. Rev. B **66**, 174201 (2002).

[59] E. E. Ferrero, S. Bustingorry, and A. B. Kolton, Phys. Rev. E **87**, 032122 (2013).

[60] L. S. Si, X. Y. Liao, and N. J. Zhou, Comput. Phys. Commun. **209**, 34 (2016).

[61] X. P. Qin, B. Zheng, and N. J. Zhou, J. Phys. A **45**, 115001 (2012).

[62] A. K. Pramanik and A. Banerjee, Phys. Rev. B **79**, 214426 (2009).

[63] A. Salazar, M. Massot, A. Oleaga, A. Pawlak, and W. Schranz, Phys. Rev. B **75**, 224428 (2007).